XXXVI Ibero-Latin American Congress on Computational Methods in Engineering
CILAMCE
Rio de Janeiro, 22-25 Nov 2015

CFD NUMERICAL MODEL DEVELOPMENT FOR FRICTION STIR WELDING OF ALUMINUM ALLOYS

Buglioni, Luciano

buglioni@inti.gob.ar

(1)

Tufaro, Leonardo

ltufaro@inti.gob.ar

(1), (2)

Svoboda, Hernán Gabriel

hsvobod@fi.uba.ar

(2), (3)

(1) Instituto Nacional de Tecnología Industrial, Centro de Investigación y Desarrollo en Mecánica, San Martín, Buenos Aires, ARGENTINA.

(2) GTSyCM3, INTECIN, Facultad de Ingeniería, Universidad de Buenos Aires, ARGENTINA.

(3) Consejo Nacional de Investigaciones Científicas y Técnicas, ARGENTINA.

Abstract. *In the present work different Computational Fluid Dynamics (CFD) models for Friction Stir Welding (FSW) of aluminum alloys were developed and studied. Experimental validation was done, for which, plates of AA5083 were butt-welded by FSW with four different conditions, varying tool rotational and travel speed. From the welding process were measured thermal cycles at different distances from the weld centerline in conjunction with axial force and energy consumption. In addition, macrographs of transversal cuts the different zones for all welding conditions have been prepared. These measures were used to calibrate models and to compare them. Proposed models, with specific input parameters, were evaluated for the different welding conditions experimentally done, and the numerical results were compared with measured variables of the process (thermal cycles, consumed power, axial force, stirred zone). Numerical input parameters used in each model (dissipation condition, heat generation mechanism, boundary conditions, etc.) were studied in order to predict its influence over model results and to find the better ones that enhance its prediction capacity. Models also have been compared between them to achieve a representative model which fulfill best match with experimental data.*

Keywords: *Friction Stir Welding, Numerical Modelling, CFD, AA5083, Plastic Flow*

1 INTRODUCTION

Different numerical models to simulate Friction Stir Welding (FSW) process have been developed over the last years (He (2014)). These models can be grouped in analytical ones (Schmidt (2007)), thermal (Tufaro (2012)), coupled thermal-structural by very different material models and formulations (Soundararajan (2005), Awang (2007)), fluid-thermal (Arora (2009), Wang (2013), Su (2015)), among several others, including combination of different ones at different process stages. These models are focused mainly in calculation of heat generation rate, residual stresses and strains, axial plunge force, thermal cycles, heat transfer and material flow.

In what concerns to CFD models, however, their testing has been mainly limited to comparison of the numerically predicted thermal cycles with the corresponding experimental data. Some recent works like Arora (2009) has been expand this testing by matching transversal thermal profiles, energy and torque. However, is not common to see all different variables together like pressures and axial force with thermal cycles and the above mentioned in order to not only match them with experimental data but also to study their variation with welding conditions.

On the other hand, CFD models have a large quantity of numerical input parameters involved, such as dissipation and friction coefficients, slip between tool and workpiece, material formulations and assumptions. These parameters are fixed to solve each specific experimental process with particular conditions, but is perhaps most interesting to consider not only these values but also how all these parameters variation affect model response and results, not only to find one model which covers one single experimental case, but also to serve as basic knowledge in order to determine which are convenient to different conditions and to the model limits.

The aim of this work was to develop different CFD Friction Stir Welding Models, and then to study the numerical parameters influence in their response, all of these in order to define a suitable and representative model taken into account different experimentally measured variables.

2 EXPERIMENTAL PROCEDURE

Several AA5083 aluminum alloy samples of 150 x 75 x 3 mm were butt welded under different conditions, using an endogenous FSW machine, according to Tufaro (2014). In Table 1 are shown welding parameters studied. Travel speed TS and rotation speed ω were varied whereas tilt angle was maintained constant.

Table 1. FSW welding parameters and probe designation

Id	Rot. Speed [rpm]	Travel Speed TS [mm/min]	Tilt [°]	Pitch $= \omega/U$ [rev.mm^{-1}]
680-73	680	73	1.5	9.3
680-98	680	98	1.5	6.9
903-73	903	73	1.5	12.4

903-98	903	98	1.5	9.2

Tool has a tapered pin with a concave shoulder and was made of H13 steel. Shoulder diameter is 12 mm and pin major and minor diameters are 4 and 3 mm, respectively. Pin length is 2.8 mm. During process were measured different process variables using a data acquisition system with 4 channels. Thermal cycles were acquired with 2 type K thermocouples (TCs), which were located as following from the weld centerline: TC1 between 7 and 8 mm and TC2 between 11 and 12 mm, inside 1 mm diameter holes at 2 mm depth. In Figure 1 the FSW experimental setup (a) and TCs position from centerline (b) are shown. Axial force was also measured using a strain gage instrumented at machine head. At last, line current (I_L) of asynchronous motor was measured, using a transducer with a sensibility of 10mV/A.

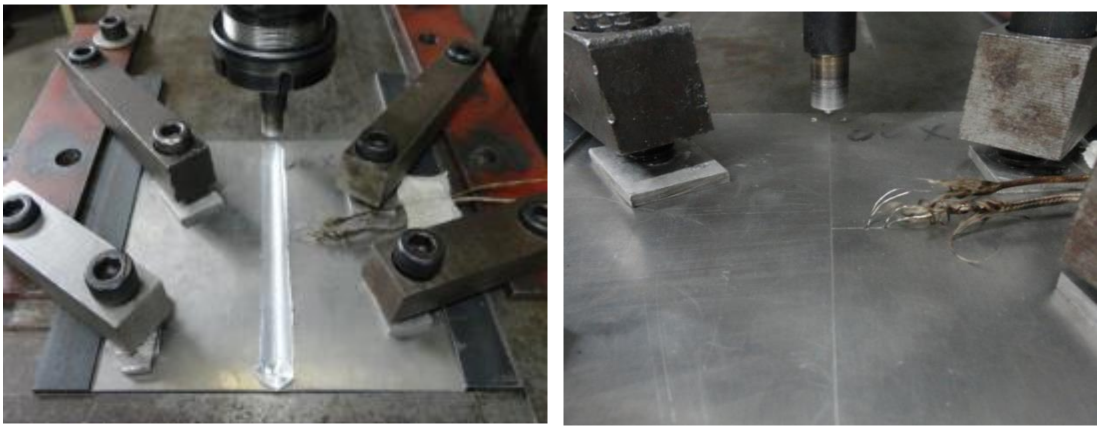

Figure 1. a. Friction stir welding (FSW) device and mounting, b. TC's locations

3 NUMERICAL MODEL

In this work, a CFD numerical model representing FSW process has been developed. Different numerical parameters were analyzed to achieve a representative model (which minimizes error against experimental measured values). Considerations made include representation of different welding parameters, taking into account both stick and slip heat generation mechanisms, a non-constant heat dissipation and a non-uniform slip between tool and workpieces.

A general numerical constitutive model has been developed in ANSYS® Fluent. It consists of a control volume of 150 mm x 150 mm x 3 mm (which includes both butt welded workpieces). This control volume domain has been represented in Fig. 2. Boundary has been divided into inlet, outlet, sides, top, tool (with different parts), and bottom, being this last subdivided into bottom-interior (below tool) and bottom exterior (beyond tool).

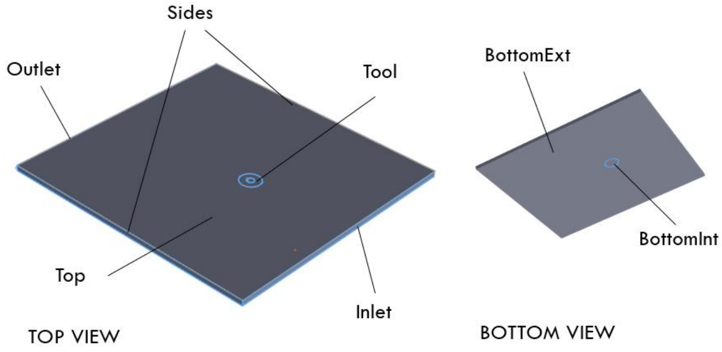

Figure 2. Numerical Domain and boundaries

This domain has a central cylindrical shaped volume which has been removed, at 60 mm from the inlet in longitudinal direction (Fig. 3a), representing welding tool, which shape has been corrected according with the tool profile, experimentally obtained. Tool dimensions are represented in Fig. 3b. Tool was sinked in workpiece in such a way to be both shoulder and workpiece top coincident at middle longitudinal point. Tool tilt angle is adopted as 1º by calculating tool bending from obtained axial force projection (Fig. 3c).

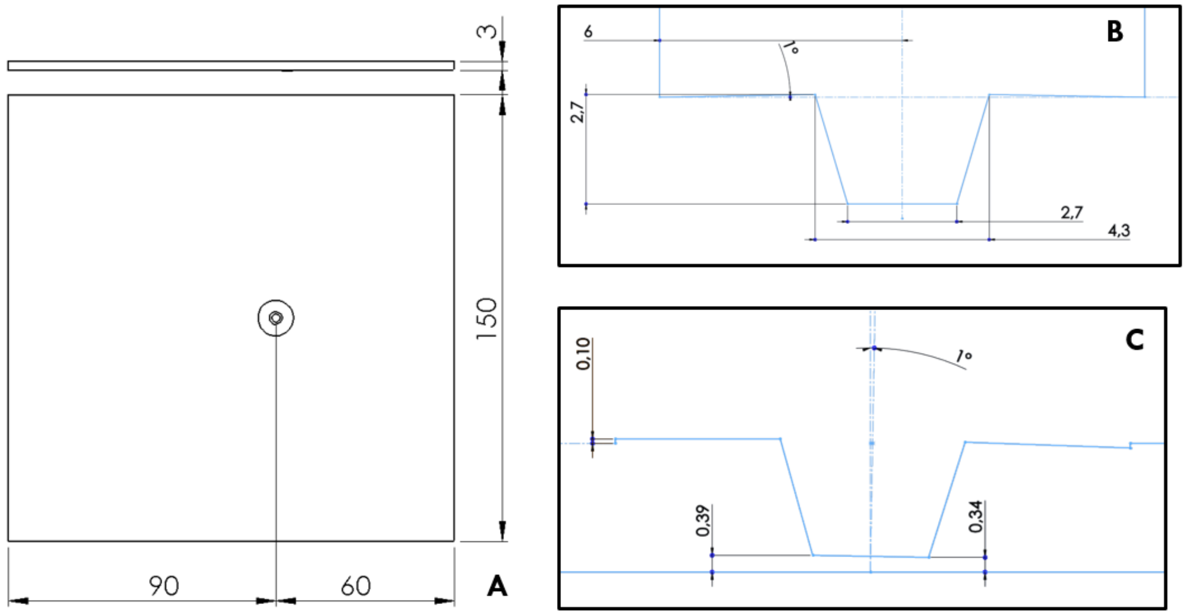

Figure 3. Domain dimensions (A), tool dimensions (B) and tool positioning (C)

Model boundary conditions are all moving walls with sliding properties (null shear stress) at top and sticking conditions at sides. At workpiece bottom, different shear stress conditions as been proposed. Outlet boundary is specifically defined as a pressure-outlet boundary type and has (as well as the velocity inlet) 300 °K which is reference temperature. Heat dissipation takes different values in several zones. Both top and sides has a convection coefficient *hc* = 30 W/m^2-°K. Dissipation value and distribution at bottom is also a numerical parameter which variation has been studied in next sections.

Mesh is shown in Fig. 4 and has about 200,000 cells, its density grows up near tool walls to account for velocity and temperature variations.

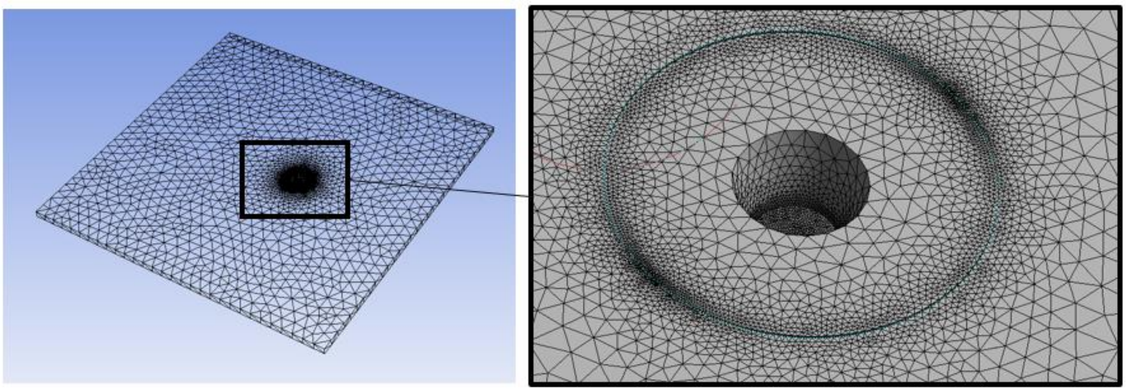

Figure 4. Domain mesh and tool mesh detail

Material model is governed by Zener–Holloman law proposed by Sheppard and Wright (1979), which describes the relationship between the temperature, strain rate $\dot{\varepsilon}$ and flow stress as follows in Eq (1) to (3):

$$\sigma = \sigma_r \operatorname{asinh}(x) \tag{1}$$

where x is defined as :

$$Z = \dot{\varepsilon} \exp\left(\frac{Q}{RT}\right) \tag{2}$$

$$x = \frac{Z}{A} \tag{3}$$

Thermal properties of 5083AA are obtained from Kim, Chung and Badarinarayan (2009) and correlated with a polynomial trending line.

3.1 Proposed numerical parameters variations

The methodology proposed for this work was to evaluate the response of different CFD models. Each model comprise was solved for four different welding conditions, and were matched with experimental data obtained from the welds produced. Finally, all these set of models are compared with another welding values measured (axial force, TC2 peak temperatures, cooling, TMAZ profile, heat values) and related with each welding condition.

In order to obtain a suitable and representative numerical model, different numerical parameters has been modified and tested by studying model response and by comparing it with experimental measures. Parameters involved in this study are: boundary conditions (BCs) of workpiece bottom, both dissipation coefficient h_c (distribution and value) and wall momentum boundary condition, slip δ between tool and workpiece, heat generation mechanisms and finally material properties related with flow stress. Another parameters has been adjusted in the development of the model and then remain fixed throughout this work, these involves tool indentation, tilt, types of meshing between tool and workpiece in zones where is a gap (there is, upstream tool-piece contact).

Study of dissipation coefficient involves different dissipation distributions and values at bottom of workpiece. Literature includes constant dissipation at the whole bottom (Tufaro,

2014) whereas some works include discontinuous dissipation, applying a greater value at the bottom of the tool due to high temperature and pressures (Wang, 2013)). Other works present a temperature dependent dissipation (Arora (2009)) or even, for Friction Stir Spot Welding processes (FSSW) a gap dependent distribution (Awang (2007)).

In what concerns to numerical against experimental adjustment, following previous works (Tufaro (2012, 2014), Buglioni (2014)), the most significant parameter to be matched is the peak temperature of thermo couple which is near to weld centerline (TC1). There are other variables to be considered in order to adjust the numerical model, these are, among others: tool axial force, peak temperatures of TC2 (which is far away from weld centerline than TC1), Thermo Mechanically Affected Zone (TMAZ) size and geometry, temperature distribution and cooling rate.

General considerations applied for all models include: null generated flux at negative pressures or shear stresses; limitation of strain rate $\dot{\varepsilon}$ in viscosity calculation, about 90% of the plastic deformation are assumed to be converted into heat (Arora (2009)); to limit maximum temperature to T_s, being this value the material solidus temperature.

3.2 Proposed Models

Model 1 considers a constant dissipation to workpiece bottom plane with a higher value below the welding tool. Regarding to heat flux generation, the contact shoulder radius ratio (CSRR) method developed by Wang (2013) was applied. This method assumes that only a certain proportion of the shoulder is in contact with the workpiece material and generates heat. For this model, heat contribution per surface area has the form presented in Eq. (4):

$$q = U_q \tau_w \eta_{pl} \tag{4}$$

where q represents heat generation per surface area, τ_w is the shear stress at the wall–tool interface according to Wang (2013). Some authors consider this value to be yield stress instead wall stress (Nandan (2006), Arora (2009)). This method has been tested but was obtained an oscillating solution. Coefficient η_{pl} means fraction of plastic energy converted to heat and is defined to 0.9 according to Arora (2009), although some authors consider another values (Mendez (2010) takes 1.0 and Chao (2003) 0.8). This model and the next one, in order to follow the work of Wang (2013), assume all generated heat goes through the working plate. Regarding to heat generation mechanism, this was simplified by omitting TS linear velocity (U_q in Eq. (4)) component in its calculation (it was considered in flux movement instead), hence:

$$U_q = \frac{\omega r \pi}{60} \tag{5}$$

Model 2 consists of the analysis of boundary and material restrictions adopted. According to some researches (Arora (2009)), it is common practice to limit maximum strain rate $\dot{\varepsilon}$ in flow stress and hence viscosity calculation, affecting the viscosity one. On the other hand, momentum boundary conditions at bottom of workpiece can be either sticking or sliding, or even a combination of two. Working with several values of $\dot{\varepsilon}$ and bottom boundary conditions, it has been found that for materials with lower $\dot{\varepsilon}$, sticking boundary condition may lead to diverging solution because of the material shear stresses at bottom (due to higher viscosities).

At the opposite, higher $\dot{\varepsilon}$ with slip (null shear) boundary conditions leads to nearly null axial forces.

In other point of view, Model 3 considers a pressure dependent dissipation configuration at bottom of workpiece with both stick and sliding heat generation mechanisms. Pressure dependent mechanism was proposed following some authors criteria (Wang (2013), Soundararajan (2005)) in which zones with low contact gap (equivalent to high pressures) has greater values of heat dissipation coefficient. Eq. (6) to (9) describe the expression for the pressure dependent dissipation.

$$h = h_{min} \qquad p < p_{min}, \;\; r > R_{min} \tag{6}$$

$$h = h_0 + k_h p \qquad p_{min} < p < p_{max} \;, \;\; r < R_{min} \tag{7}$$

$$h = h_{max} \qquad p_{max} < p, r < R_{min} \tag{8}$$

In previous equations, R_{min} is an arbitrary bottom radius defining domain, p is the pressure, h_0 means minimum dissipation coefficient (taken as 300 W/m^2-°K). $h_{max}, h_{min}, p_{max}$ and p_{min} are dissipation coefficient and pressure limitations in order to reach convergence, and k_h is the function slope, calculated as follows:

$$k_h = \frac{h_{max} - h_{min}}{p_{max} - p_{min}} \tag{9}$$

This model adopts same material of first model ($\dot{\varepsilon}_{min} = 1$) wit stick boundary conditions at workpiece bottom. Taken into account both stick and slide phenomena, the heat flux per area can be represented by Eq. (8).

$$q = \eta_c\big((1 - \delta) U_q \tau_w \eta_{pl} + \delta \mu p U_q\big) \tag{10}$$

In this equation, δ is slip rate, η_c represents heat flux fraction which goes through workpiece (conduction efficiency, taken as 0.95 according to Chao (2003), although can be lower according to some authors (Lohwasser (2009) takes 0.7 to 0.9 and Dickerson (2003) 0.9), μ is friction coefficient and p is the pressure. Following Arora (2009), slip rate and friction coefficient have the form:

$$\delta = \delta_1 + \delta_2 \left[1 - \exp\left(-\delta_0 \frac{\omega}{\omega_0} \frac{r}{R_s}\right)\right] \tag{11}$$

$$\mu = \mu_0 \exp\left(-\delta \frac{\omega}{\omega_0} \frac{r}{R_s}\right) \tag{12}$$

where δ_0, δ_1 and δ_2 are adjust parameters, ω is tool rotation speed whereas ω_0 is the reference value for this, taken as 400 rpm, r is the radius of the fluid cell R_s is the radius of the tool shoulder.

Last model, Model 4, considers slip conditions at both external and internal bottom boundaries. It also includes a CSRR, and, the aim for this model, is to be a conjunction between Model 2 and 3, modifying BCs and material respect to Model 3 to account for slip heat generation to distinguish from model 2. Table 2 resumes all models described above.

Table 2. Proposed models

Id	Stick Heat	Slide Heat	Slip Params $\delta_0 - \delta_1 - \delta_2$	CSRR	$\dot{\varepsilon}_{min}$	BotInt BC	BotExt BC	Bot h_c Type	Bot h_c Ext - Int Val
1	Yes	No	-	68	1	Stick	Stick	Const	300 – 8800
2	Yes	No	-	68	0.01	Null τ	Null τ	Const	300 – 8800
3	Yes	Yes	4-0.2-0.6	100	1	Stick	Stick	$f(p)$	300 - $h(p)$
4	Yes	Yes	3-0.1-0.8	90	0.01	Null τ	Null τ	Const	200 – 200

Figure 5 describes slip rate distribution along tool radius (left) for all models. At right is shown a value which gives some idea about the amount of average tool slip, integrated slip, which is obtained as follows:

$$I_s = \frac{\int_0^R \delta dr}{R} \tag{13}$$

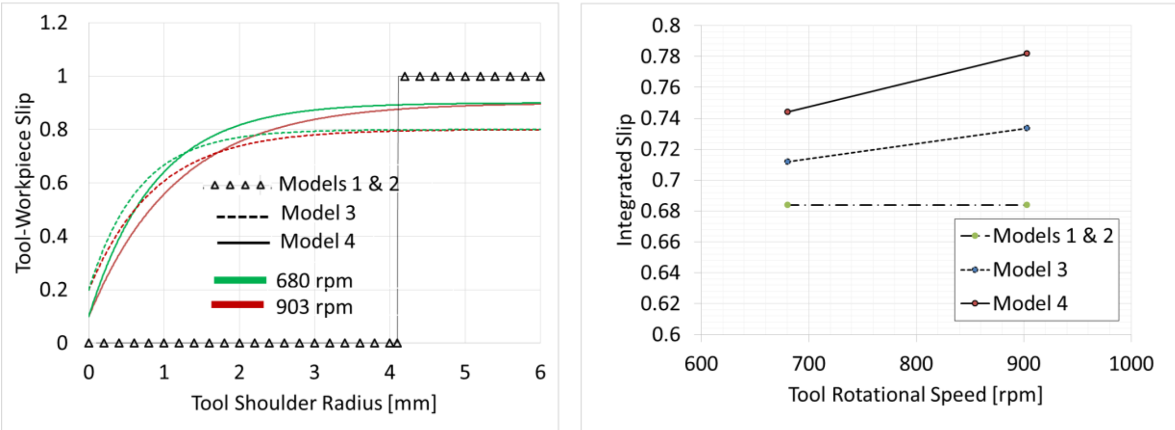

Figure 5. Slip rate variation inside tool (left) and Integrated slip vs. rpm for all Models

From the figure can be seen Model 1 having an independent slip rate with rpms, whereas Model 3 has a greater sticking condition that model 4, which is the most sliding one. Also the variation with rpm is greater. This lower sticking of Model 4 will lead, as seen later, to small heat generation and this explains why thermal dissipation (Table 2) of this model is too small.

4 RESULTS

In this section are shown the results obtained both from experiments and from all presented models.

4.1 Model adjustment

Figure 6 shows numerical and experimental thermal cycles for Model 1. As was described above, TC1 is matched for 680-73 condition. It is observed that for 680-98 temperature of this TC is very well matched, whereas for faster tool rotation speed values numerical results are overestimated. Regarding to TC2, it seen numerical peak temperature below experimental one for slow tool rotation speeds and for faster ones it is observed the same phenomena that in TC1. These observations concerning to heat flux overestimation for high tool rotational speeds are in concordance with Wang (2013). To solve this, author has introduced material softening at high temperatures in comparison with tool-workpiece slip mechanism, however, these models does not account for sliding generated heat fluxes. Models 3 and 4 will introduce this slip mechanism in conjunction with sliding heat flux.

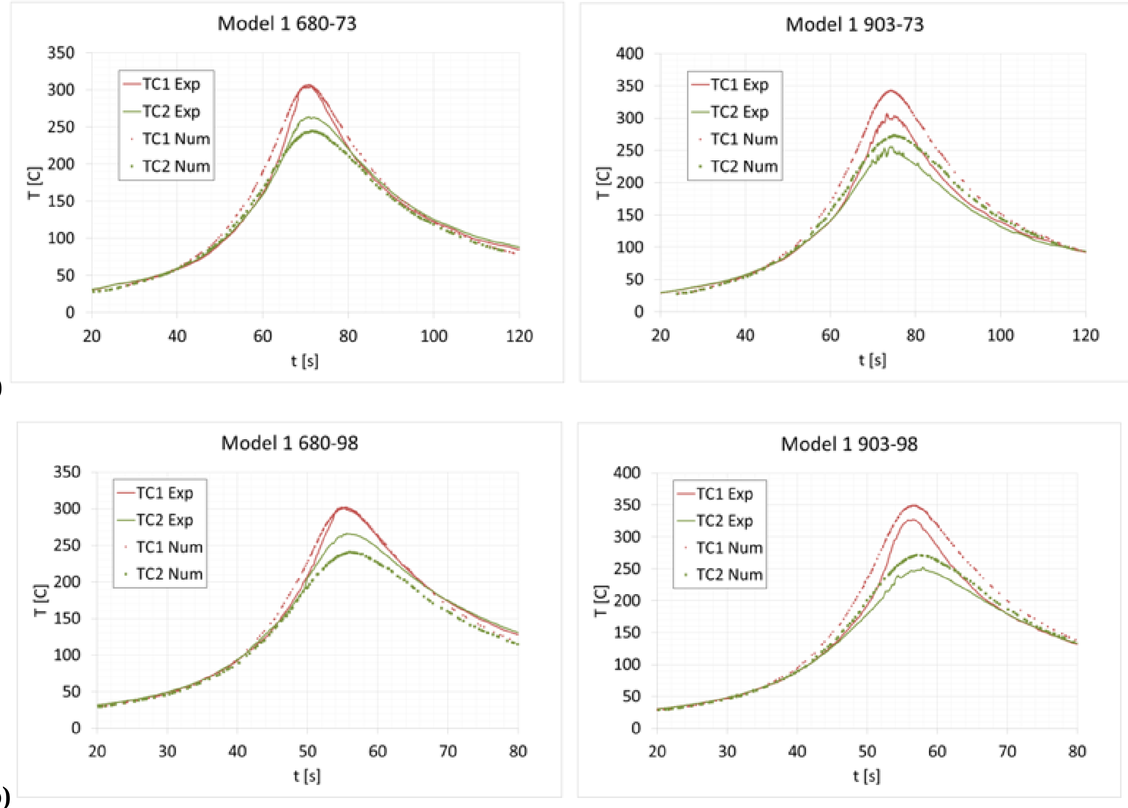

a)

b)

Figure 6. Thermal cycles for Model 1: a) 73 mm/min, b) 908 mm/min

Figure 7 shows axial force and sticking torque against travel speed, for 680 and 903 rpm. Regarding to experimental values, as this process has not been made with control of position, and knowing influence of tool position with this variable, resulting values should be taken as an approximation. It can be seen that sticking torque drops with rotational speed whereas it remains near a constant value with TS variations. This drop in sticking torque could be related to material softening (represented by viscosity decreasing) with temperature.

In results shown, axial force does not decrease with rpm for this model as may be expected due to viscosity decreasing with temperature, and this may be related to the model assumptions about confined control volume, and restrictions to material minimum strain rate value in conjunction with fixed non-slip boundary conditions. Another issue to consider is axial force increasing with TS, which is reported in different works (Su (2015)). As seen later, this is related to material properties and boundary conditions.

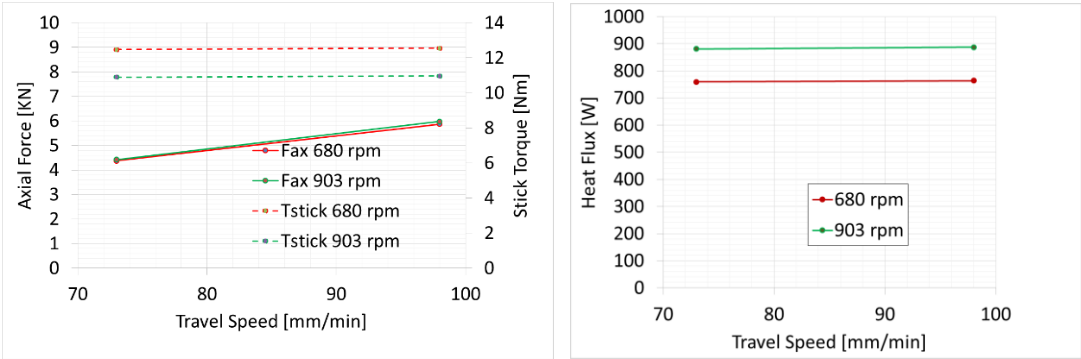

Figure 7. Axial force, Stick Torque and Heat Flux vs. TS for Model 1

Figure 8 shows a transversal cutting plane comparing numerical constant viscosity model result ($7 \times 10^6\ Pa.s$) against Welding Nugget (WN, re-crystallized stirred area). In all transversal cuts of this work Advancing Side will be shown at left. This methodology of correlating stirred zone with material viscosity is found in Arora (2009). Some works refers to other values (line $5 \times 10^6\ Pa.s$ in Nandan (2006)). From the viscosity comparison, it can be observed a difference due to velocity and heat flux restriction CSRR. This model does not consider any form of heat flux reduction (such as slip or linear softening). It is observed a small increasing of WN in 903 rpm models, in conjunction with very high temperatures.

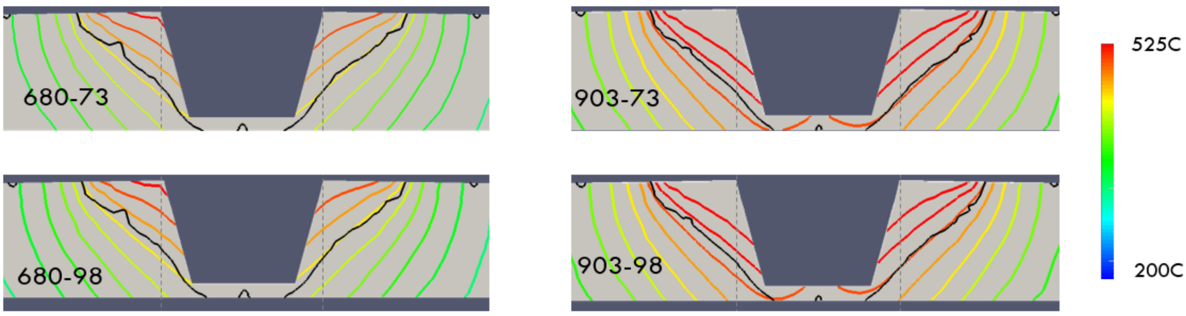

Figure 8. Thermal profile and isoviscosity (7x10[6]) contours for Model 1. Advancing side at left

Figure 9 shows a transversal cutting plane comparing numerical obtained isoviscosity previously shown against Welding Nugget (WN, re-crystallized area). It is clearly observed the impact of CSRR coefficient in the numerical model, being the stirred zone narrower than experimental. However, for 903 models (especially 903-78), is seen a large stirring zone near pin, compared with experimental. This agrees with the high heat flux generation for those models.

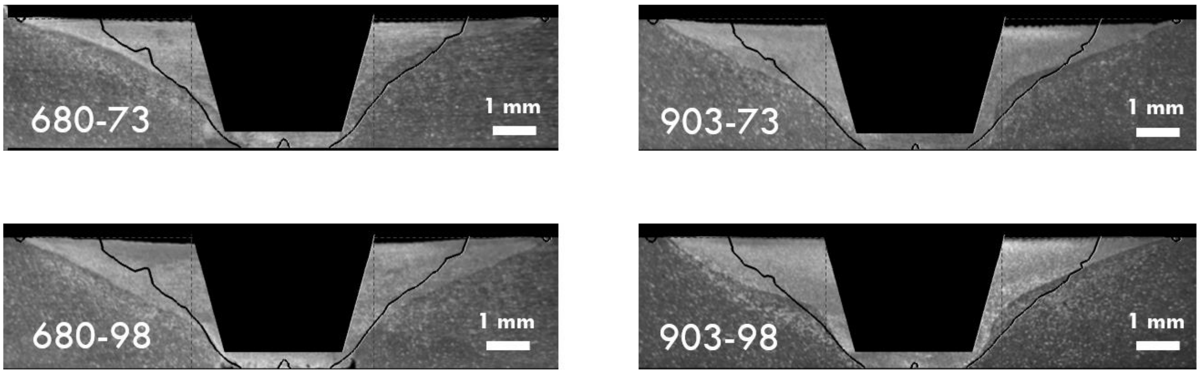

Figure 9. Isoviscosity ($7x10^6$) contours vs. WN for Model 1

Model 2 thermal cycles are shown in Fig 1 0. It is observed same behavior that Model 1. This is due to resulting Heat Flux is nearly the same as previous and dissipation coefficients are the same.

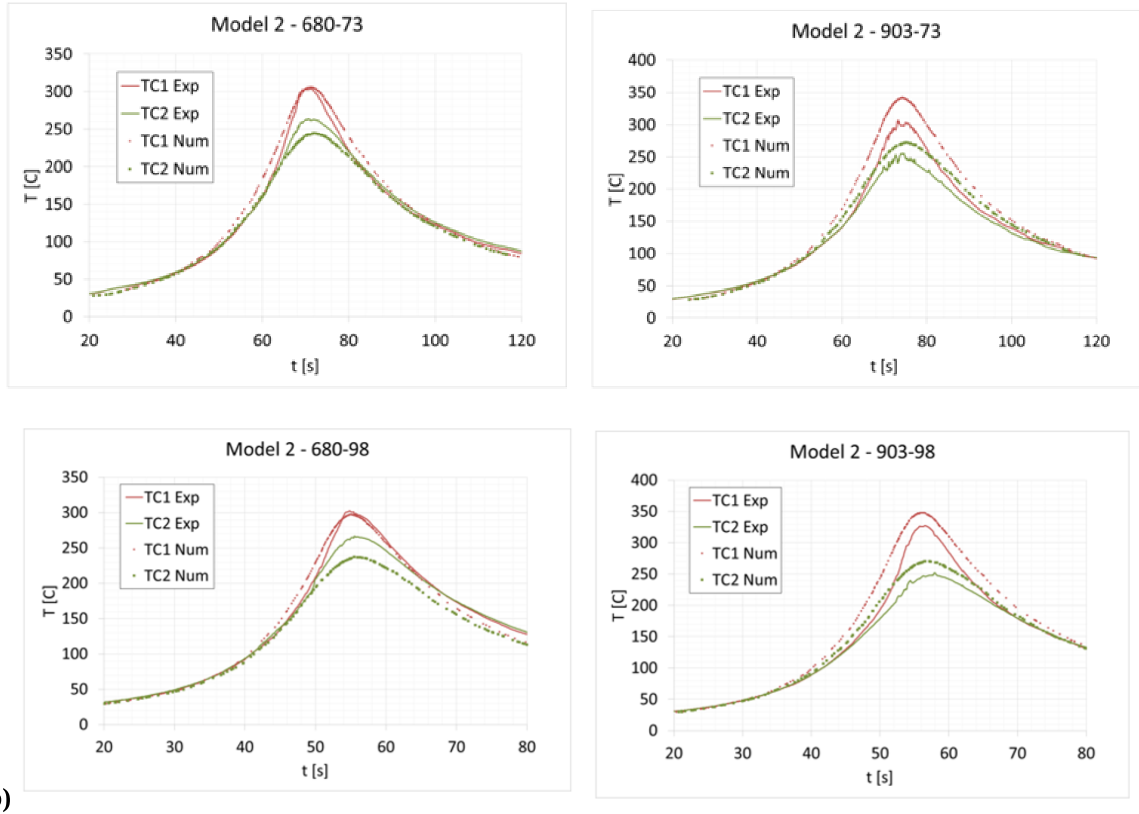

a)

b)

Figure 10. b) Thermal cycles for Model 2: a- 73 mm/min, b- 98 mm/min

Figure 11 shows Axial force and Sticking Torque against travel speed. It is observed a constant torque, with values similar to those obtained from previous model. Regarding to Axial force, it is interesting to note that whereas previous model presents similar values for both rotational velocities, this model, only with material strain rate limitation and boundary conditions modified, shows a decreasing in force response with rpm. In first model values are very similar and slightly larger for high rpm.

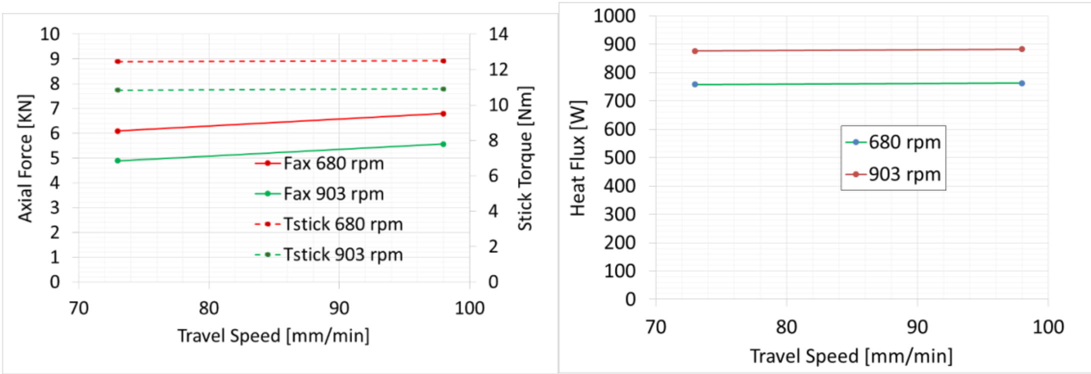

Figure 11. Axial force, Stick Torque and Heat Flux for Model 2

Figure 12 details isoviscosity contours vs. numerical thermal profiles. As in previous models, it is observed very high temperatures inside WN. Also, isoviscosity contours show a non continuous zone below tool pin. This is due to null shear boundary conditions.

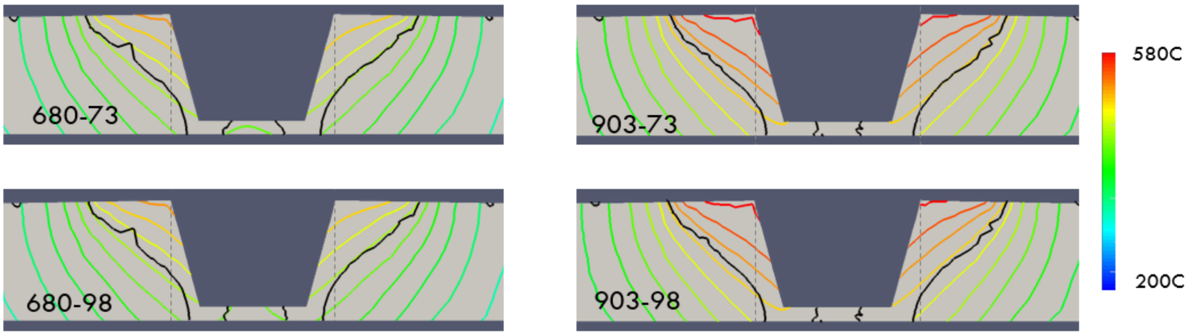

Figure 12. Isoviscosity ($7x10^6$) vs. thermal profiles for Model 2

Figure 13 compares isoviscosity against WN for Model 2. Respect to previous model, it is observed a difference at bottom of isoviscosity lines, due to change in boundary conditions. General size does not change much between models. In next section will be shown a quantitative comparison between all of them.

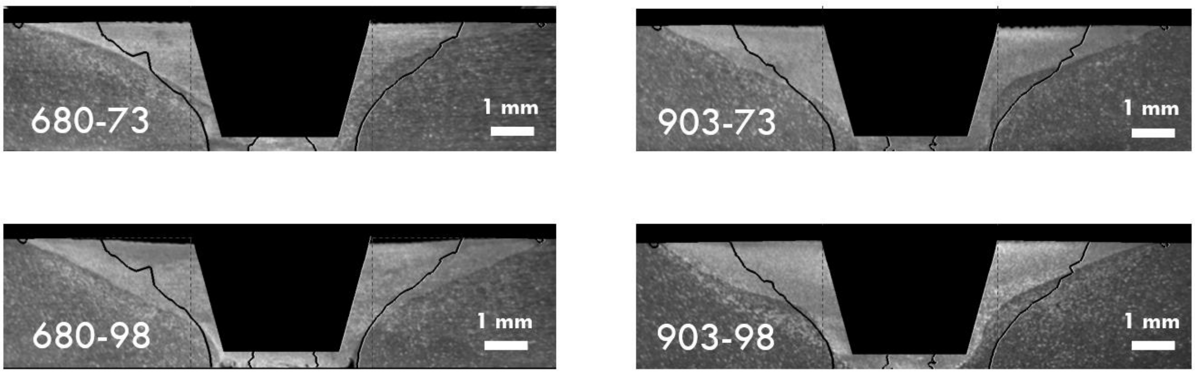

Figure 13. Isoviscosity ($7x10^6$) contours vs. WN for Model 2

Model 3 thermal cycles are shown in the following figure. It can be seen that for large TS maximum temperature at TC1 adjusts better than which obtained from constant dissipation models. This is due to the axial force dependent dissipation coefficient, which grows with TS.

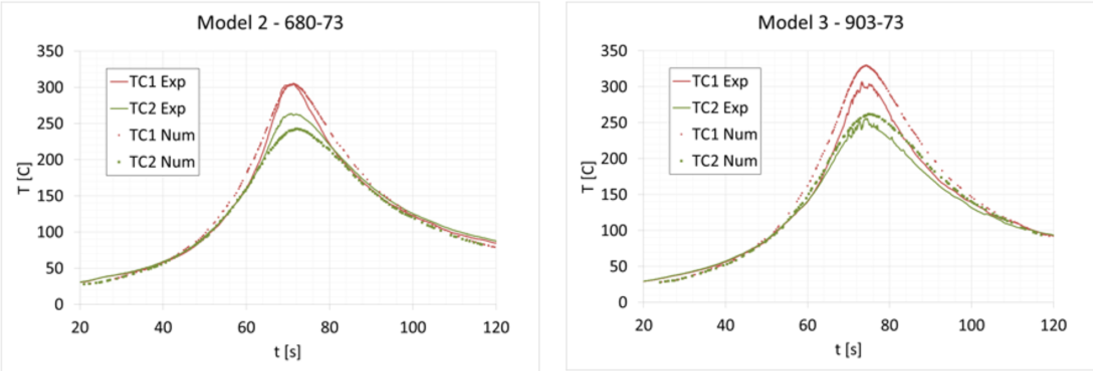

a)

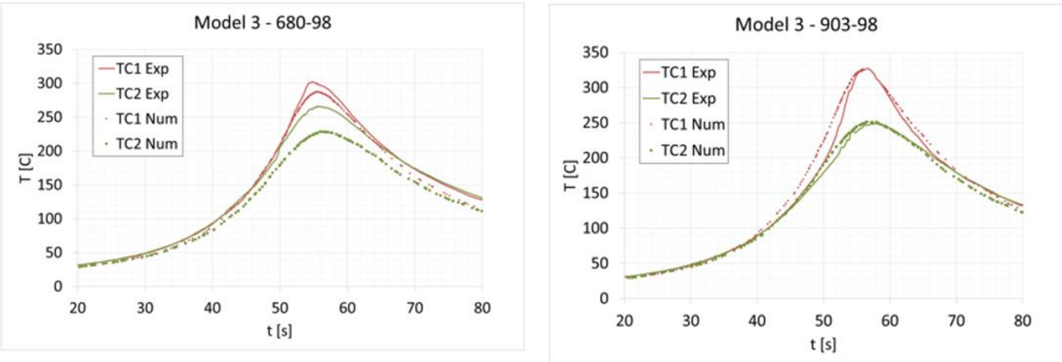

b)

Figure 14. Thermal cycles for Model 3 a) 73 mm/min, b) 98 mm/min

Figure 15 shows axial force and total heat flux against travel speed for Model 3. Again, with a more limited strain rate and sticking boundary conditions, it is observed a similar behaviour than Model 1.

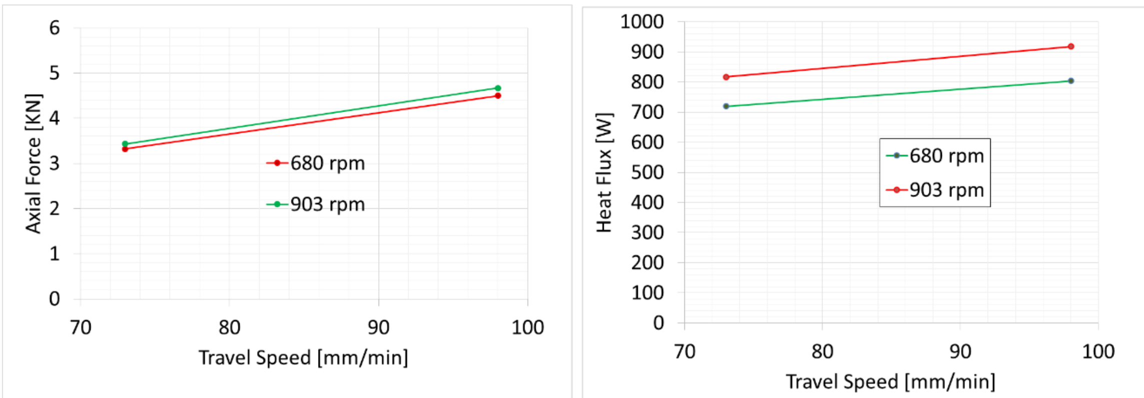

Figure 15. Tool Axial Force and Heat Flux for Model 3

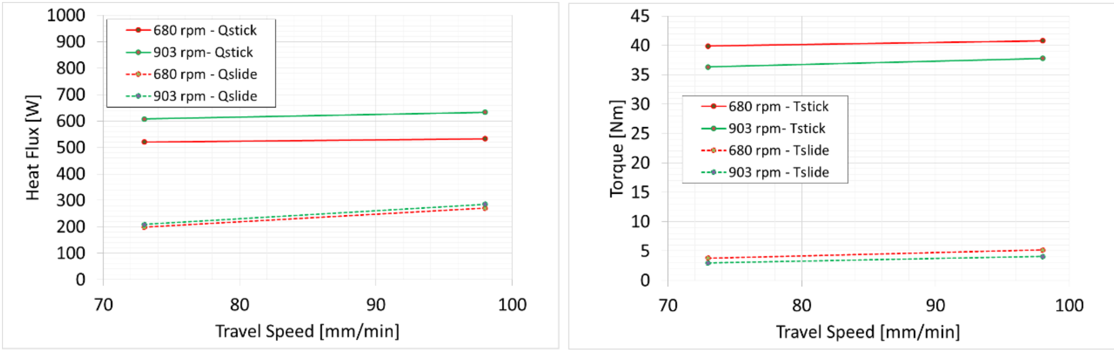

Figure 16. Sticking vs. Sliding Heat Flux and Torque for Model 3

Figure 17 shows isoviscosity and thermal profiles. At first sight is noted a more reallystic peak temperatures near tool, too far below to which reached in previous models. This is due to dissipation increase at this zone.

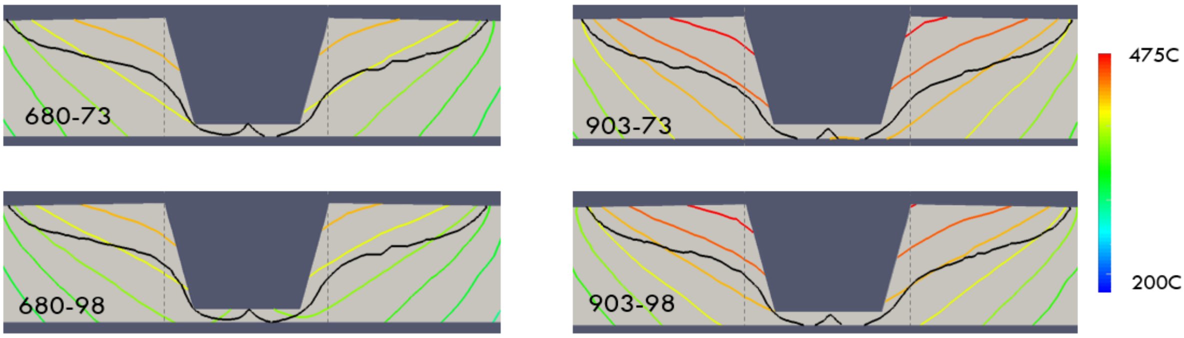

Figure 17. Isoviscosity (7x10^6) vs. thermal profiles for Model 3

Figure 18 shows experimental WN vs. constant viscosity numerically obtained. It is observed a better agreement between them in comparison with previous models.

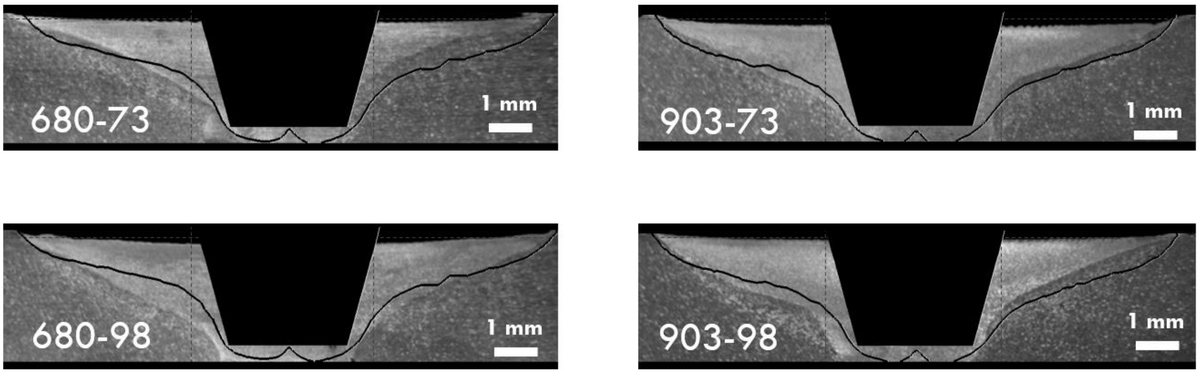

Figure 18. Isoviscosity (7x10^6) contours vs. WN for Model 3

Figure 19 shows thermal cycles for Model 4. It can be seen an important improvement of peak temperatures adjustment, in all models, being the exception TC2 for slow rpm.

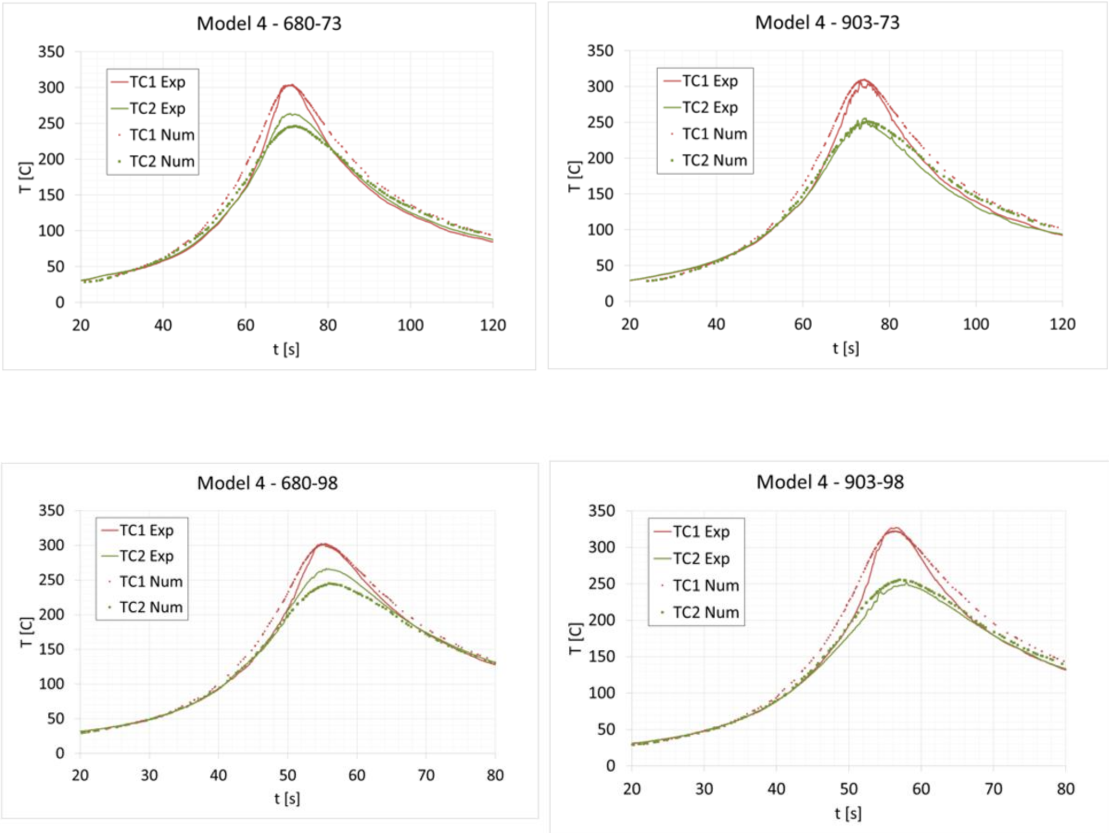

a)

b)

Figure 19. Thermal cycles for Model 4

Figure 20 shows axial force and heat flux at tool-workpiece interface for Model 4. Axial force response against TS is the same for both rotation velocities, increasing with TS increase. At first attempt, is observed a low axial force variation with TS, like in Model 2. Axial force difference between 680 and 903 rpm is oposite than Model 3, being higher for slower rotational velocity. Total heat Flux is lower than Model 3. Heat flux is slightly lower than the other models. This is important to note here that new models with same boundary conditions and materials are being developed, with different slip distributions resulting on a notable higher heat generation values, comparable to these models. In other words, this lower heat flux is mainly due to slip distribution. However, models response regarding to peak temperatures with all welding conditions do not match as well as this model.

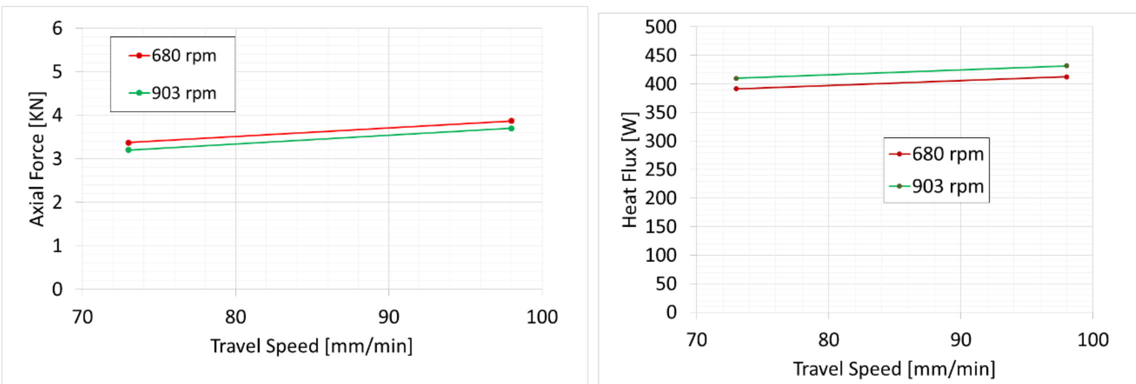

Figure 20. Tool Axial Force and Heat Flux for Model 4

Figure 21 compares sticking and sliding heat fluxes for Model 4. It can be seet that sticking mechanism is predominant, twice higher. In previous model difference was greater. In addition, sticking heat flux diminish with TS whereas in previous mdel remain constant. This response is probably caused by slipping rate since model 2 with same material and boundary conditions presented a constant heat flux with TS variation.

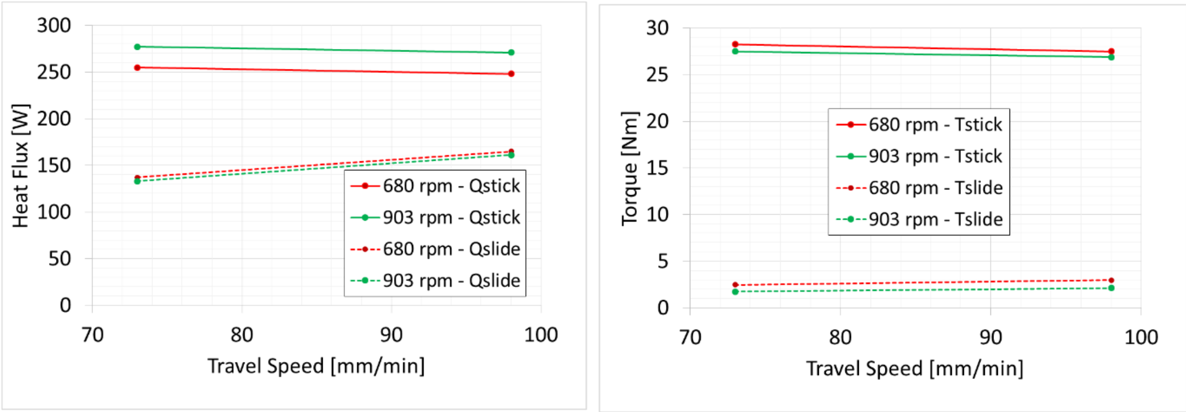

Figure 21. Thermal profile and isoviscosity (7x106) contours for Model 4

Figure 22 shows temperature distribution against isoviscosity contours. It is observed than temperatures differs from about 50º with previous models. This difference regards on low heat flux, but is mainly related to balance between heat dissipation value from above tool and heat flux on top (tool heat generation). It was observed, by testing different developed models, that this balance affects also to isotemperatures shapes, being these in near an horizontal distribution for high cooling rates at bottom and in a more vertical position for lower values. In this model, due to lower isotemperatures are crossing isoviscosity lines outside pin, being more similar near it.

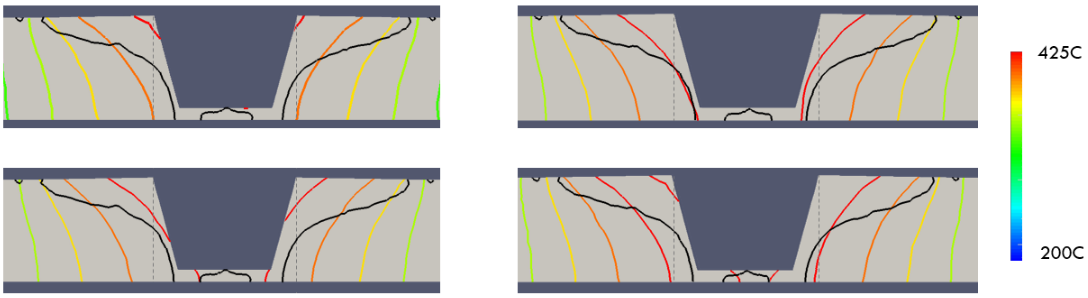

Figure 22. Thermal profile and isoviscosity (7x10^6) contours for Model 4

Figure 23 shows isoviscosity lines vs. WN macrographies. As first observation, can be said that the 90% of R_S CSRR applied, causes a good match between isoviscosity and WN boundary.

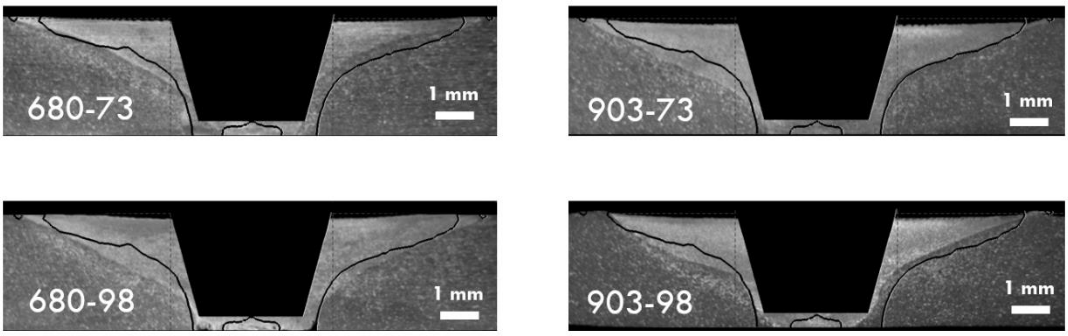

Figure 23. Isoviscosity (7x10^6) contours vs. macrographs for Model 4

4.2 COMPARISON BETWEEN MODELS

Figure 24 resumes TC1 and TC2 error sum for each welding conditions of each model set. These error sums are made overall welding conditions for each set, for each TC. It is observed a good evolution with parameters changes, being Model 4 which present minimum errors. This is due to small changes in heat flux in conjunction with constant dissipation assumption.

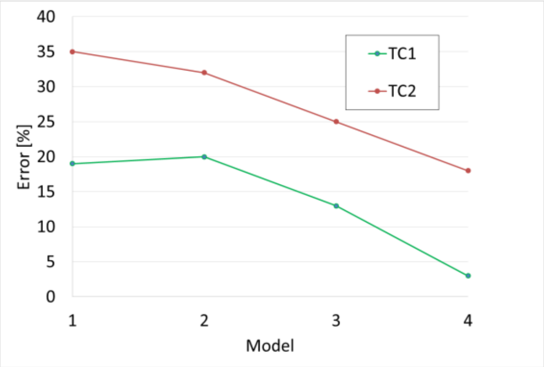

Figure 24. Thermocouples Peak Temperature error sum for all conditions

Figure 25 presents variations of WN area against pitch for all models. It can be seen that for models with sticking generated heat, rpm rising results in greater stirring areas, as expected. Model 2, which has lesser $\dot{\varepsilon}_{min}$ restriction and null shear at bottom, presents smoother variation.

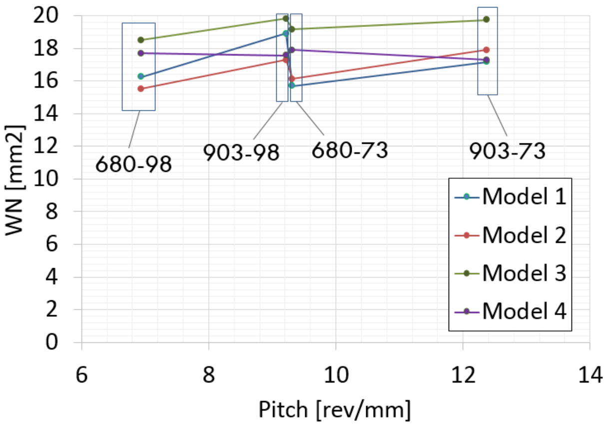

Figure 25. Welding Nugget Area vs. Pitch for all Models

Figure 26 shows at left energy per length unit consumed by the working machine vs. the same energy obtained from models, both against pitch. The former were obtained by Tufaro (2014). From these values it can be thought a constant overall efficiency. At right they are shown these same values by groups. The first one (Fig 26 a.) comprises Models 1 (which has the same values of Model 2) to 3 with the measured value affected by a constant efficiency of 21%, whereas second groups is formed by Model 4 with measured value affected by a constant efficiency of 43%. These arbitrary efficiency values have the aim to show how this numerical heat variation matches with a constant efficiency energy consumption process.

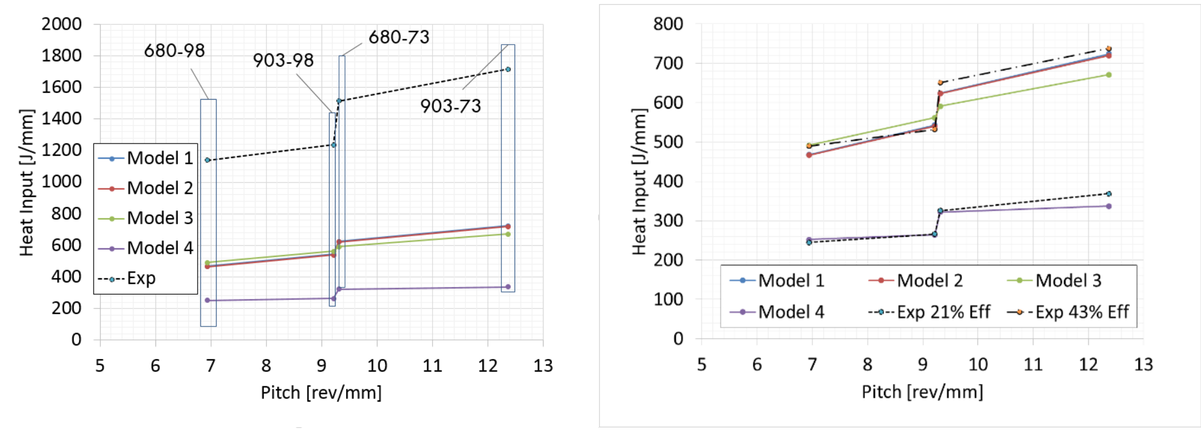

Figure 26. Heat Input vs. Pitch for all Models

Between previous figures and thermal cycles, specifically for 903-73 condition, it is observed that while Model 4 matches peak temperature, it shows low heat flux (as dissipation is minimum) assuming a constant process efficiency. On the other hand, other models show correct heat flux but peak temperatures are above experimental ones. It seem that either process efficiency is not constant, decreasing with rpm for slow TS, or slip rate decrease with rpm, or even experimental measures of 903-73 could be overestimated.

Figure 27 shows axial force against pitch experimentally measured and calculated from models. As said before for similar rotation speeds (i.e., only modifying TS), models with limited strain rate material and bottom sticking BCs (lower viscosity material, Models 1 and 3) show higher axial force variation than Models 2 and 4, however, present a significant difference with tool rotational speed changes (at constant TS), being higher at lower speed. Opposite to this, Models 2 and 4 present lower changes changing TS but they decrease its axial force values at higher rotational velocities. This difference is more important with a higher sticking condition like in Model 4. Experimental values should be taken as approximations due to the high influence of tilt and tool position with them. In all cases however, numerical axial force is lower than experimental, which suggest to sink tool shoulder furthermore.

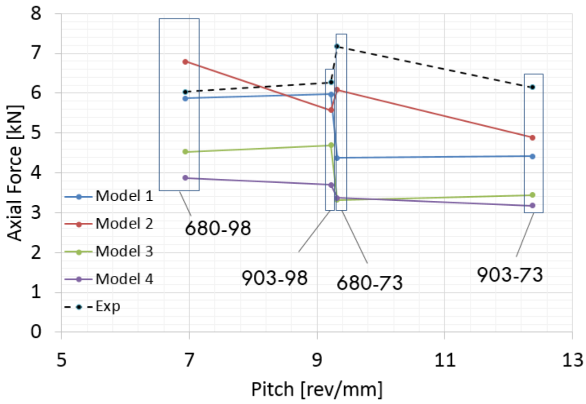

Figure 27. Axial Force vs. Pitch for All models and measured values

5 CONCLUSIONS

In this work four different CFD models have been developed and studied under different welding conditions. Numerical results were compared with the experimental measurements. Finally, a comparison between them has been made.

It has been seen that regarding to experimental peak temperatures agreement, Model 1 to Model 4 go through null-error convergence. This is perhaps experimental temperatures, specifically the 903 rpm set, have a very low variation between them, and last models would present a small variation in balance between heat generation flux and dissipation.

Heat generation and heat input mechanism is a variable very difficult to match due to be unknown the overall efficiency of the process. As was said, other models like Model 4 are being developed, with different slip distributions resulting on a higher heat generation values, comparable to these models. Above and beyond heat values, assuming a constant value, variations of heat input are a very good match with experimental data.

Regarding to axial force, all models developed show values below experimental measures, this response can be highly influenced by tool global position and model assumptions, being the former one affected in turn by indentation as much as tilt. Axial force tends to increase for a high viscosity model (less strain rate limit) and with a higher sticking condition between tool and workpiece, although this material shows lower variations with TS and rotation, and higher ones with tool rotational speed. In some cases (such as between Models 1 and 2), change only in boundary conditions and materials, affects axial force.

According to stirred zone, there has been a good match between experimental and calculated results, mainly in last two models.

As future work, it is of interest to develop a model which considers both bottom variable shear force in conjunction with top free at workpiece bottom interface, this can affect axial loads for a more realistic strain rate profile. It is of interest to modify tool position and tilt remaining constant all other parameters to see how this affects to results.

Acknowledgements

Authors wish to acknowledge INTI-Mecánica and Universidad de Buenos Aires for the funding and the use if their facilities in order to develop this work, as well as INTI-Mecánica and FIUBA-LAME personnel to the assistance proffered.

REFERENCES

Arora, A., Nandan, R., & Reynolds, A.P. and DebRoy T., 2009. Torque, power requirement and stir zone geometry in friction stir welding through modeling and experiments. *Scripta Materialia*, vol. 60, pp. 13-16.

Awang, M., 2007. Simulation of Friction Stir Spot Welding (FSSW) Process: Study of Friction Phenomena. PhD thesis, University of West Virginia.

Buglioni, L., Tufaro, L.N., & Svoboda, H.G., 2014. Thermal Cycles and Residual Stresses in FSW of Aluminum Alloys: Experimental Measurements and Numerical Models. *Procedia Materials Science,* vol. 9, pp. 87-96.

Chao, Y., Qi, X., & Tang, W., 2003. Heat Transfer in Friction Stir Welding Experimental and Numerical Studies. *Transactions of the ASME*, vol. 125, p. 138-145.

Dickerson, T., Shi, Q., & Shercliff, H., 2003. Heat Flow into Friction Stir Welding Tools, *Proceeding of the 4th International Symposium on Friction Stir Welding, Park City, Utah.*

He, X., Gu F., Ball A., 2014. A review of numerical analysis of friction stir welding. *Progress in Material Science*, vol. 65, pp. 1-66.

Kim, D., Chung, K., & Badarinarayan H., 2009. An experimental and Numerical Approach to Evaluate the Effect of Welding Conditions on Temperature during Friction Stir Spot Welding. In David S.A., DebRoy T., Dupont J.N., Koseki T., Smart H.B. eds., *Trends in Welding Research Proceeding of the 8th International Conference*, pp. 60-66. ASM International.

Lohwasser, D., & Chen, Z., 2009. *Friction Stir Welding - From basics to applications*. Woodhead Publishing Limited.

Mendez, P. F., Karem E.T., & Lienert T.J., 2010. Scaling of coupled heat transfer and plastic deformation around the pin in friction stir welding. *Acta Materialia*, vol. 58, pp. 6012-6026.

Nandan, R., Roy, G.G., & Debroy, T., 2006. Numerical Numerical Simulation of Three Dimensional Heat Transfer. *Metallurgical and Materials Transactions A, Vol. 37 A, pp.1247-1259.*

Sheppard, T., & Wright, D.S., 1979. Determination of flowstress. Part 1: Constitutive equation for aluminium-alloys at elevated temperature. Metals Technology, vol. 6, pp. 215-23.

Schmidt, H., Hattel, J., & Wert, J., 2004. An analytical model for the heat generation in friction stir welding. *Modelling Simul. Mater. Sci. Eng.* vol. 12,pp. 143–157.

Soundararajan, V., Zekovic, S., & Kovacevic, R., 2005. Thermo-mechanical model with adaptive boundary conditions for friction stir welding of Al 6061. *International Journal of Machine Tools & Manufacture*, vol. 45, pp. 1577-1587.

Su, H., Wu, C. S., Bachmann, M., Rethmeier, M., 2015. Numerical modeling for the effect of pin profiles on thermal and material flow characteristics in friction stir welding. *Materials and Design*, vol. 77, pp. 114-125.

Tufaro, L. N., Svoboda, H. G., 2012. Study of Acquired Thermal Cycles during FSW by Analytical and Numerical Models. *XXXVIII CONSOLDA – Congresso Nacional de Soldagem.*

Tufaro, L.N., Buglioni, L., Svoboda, H. G., 2014. Analysis of Axial Load and Consumed Power during Friction Stir Welding (FSW) of Aluminum Alloys). *XL CONSOLDA – Congresso Nacional de Soldagem.*

Wang, H., Colegrove, P.A., & dos Santos, J.F., 2013. Numerical investigation of the tool contact condition during friction stir welding of aerospace aluminium alloy. *Computational Materials Science*, vol. 71, pp. 101-108.